Tutorial

Tilman Glaser*

High-end spectroscopic diffraction gratings: design and manufacturing

Abstract: Diffraction gratings are key components for spectroscopic systems. For high-end applications, they have to meet advanced requirements as, e.g., maximum efficiency, lowest possible scattered light level, high numerical aperture, and minimal aberrations. Diffraction gratings are demanded to allow spectrometer designs with highest resolution, a maximal étendue, and minimal stray light, built within a minimal volume. This tutorial is intended to provide an overview of different high-end spectroscopic gratings, their theoretical design and manufacturing technologies.

Keywords: Carl gratings; concave aberration-corrected gratings; diffraction efficiency; diffraction gratings; interference lithography; replication; scattering; stray light; volume holographic gratings.

OCIS codes: (050.1950) Diffraction gratings; (050.2770) Gratings; (220.3740) Lithography; (090.2890) Holographic optical elements; (220.4241) Nanostructure fabrication; (230.4000) Microstructure fabrication; (290.2648) Stray light; (220.1000) Aberration compensation; (090.7330) Volume gratings; (240.6490) Spectroscopy, surface.

DOI 10.1515/aot-2014-0063
Received November 21, 2014; accepted January 8, 2015

1 Introduction

History of diffraction gratings starts with Rittenhouse [1], who arranged parallel hairs in the threads of fine screws to investigate more precisely the physical background of the observed diffraction image of a lamp. He was asked by a friend to explain the picture shown in Figure 1.

Milestones in the development of spectroscopic gratings are mechanically *ruled* gratings with high resolution by Fraunhofer in 1821, the invention of *concave* gratings by Rowland in 1881, and the design of *concave aberration corrected* gratings starting in the 1970s. They will be shortly discussed in the following sections.

So, until the end of the 19th century, only plane gratings were used. A spectrometer based on a plane grating requires additional optical elements to image the slit to the detector. Optimization of all these optical elements allows to minimize the total aberrations of a spectrometer.

Gratings made a significant step forward, when Rowland began to rule gratings on concave substrates and thus manufactured *imaging gratings*. Especially UV wavelength region losses could be drastically reduced when the entire spectrometer consisted only of one single optical element: the imaging grating. Unfortunately, only coma aberration correction was possible. The radius of the substrate had to be rather large, in an order of some hundred millimeters to some meters, independently, if these gratings were mechanically ruled or, later, manufactured by interference lithography (IFL) using collimated light waves. As slit and detector had to be placed on the Rowland circle with a diameter equal to the substrate radius, such spectrometers were quite large.

It was a next important milestone when concave aberration-corrected gratings, including Offner gratings, could be manufactured by IFL using point sources. Not only stronger curved substrates with corresponding short focal lengths could be used but also a much better aberration correction became possible. Using convergent and divergent waves counterpropagating through the substrate from both sides, a blazed grating profile and, thus, enhanced diffraction efficiencies could be realized. These gratings, used in reflection mode, are known to satisfy the highest spectroscopic demands.

For such *c*oncave *a*berration-co*r*rected gratings or even more general *c*urved *a*berration-co*r*rected gratings made by interference *l*ithography, the acronym Carl gratings is used in this tutorial.

***Corresponding author: Tilman Glaser,** Microstructured Optics/Grating Production, Carl Zeiss Jena GmbH, Carl-Zeiss-Promenade 10, 07745 Jena, Germany, e-mail: tilman.glaser@zeiss.com

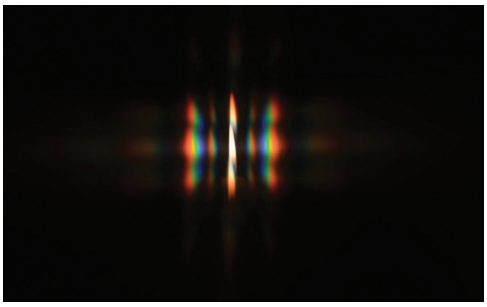

Figure 1 Picture of a candle. Observed from a few meters behind, looking through a silk handkerchief.

There are countless contributions from many ingenious scientists. Only a few examples of parameters from their designed ruling engines, manufactured gratings, or theoretical contributions can be cited in the next sections. For a fundamental discussion refer to excellent reviews and books as Stroke [2], Chrisp [3], Born and Wolf [4], and Loewen and Popov [5].

The nomenclature of polarization and diffraction order numbering is shown in Figure 2.

Phase relations determining the grating equation

$$\Lambda \cdot \sin\theta_{inc} + \Lambda \cdot \sin\theta_{out} = m \cdot \lambda$$

can also be identified from Figure 2, with the grating period Λ, the wavelength λ, the angles of incidence θ_{inc}, and of reflection θ_{out}, and the diffraction order number m.

Exciting developments emerging from the application of gratings outside spectrometry, such as chirped pulse amplification, photonic crystals, metamaterials, and many other applications shall not be treated here, neither details on their manufacturing technology.

2 Grating types

High-end spectroscopic diffraction gratings typically use *blazed* or *sinusoidal* surface profiles.

Only in rare cases lamellar or trapezoidal surface profiles are advantageous – these profiles may result from a rigorous profile optimization when additional requirements must be met, such as polarization independence over a larger wavelength range or suppression of undesired diffraction orders under a specified level.

After the introduction of typical surface-corrugated grating profiles the differences compared to volume holographic gratings are presented.

Grating types superior for spectroscopic applications will then be discussed.

Classifications such as thin, thick, and intermediate gratings reflect the demand to understand the diffraction behavior from a physical point of view, and to describe the diffraction behavior using analytical equations – avoiding the necessity to solve rigorous numerical models hiding the physics behind. Although these technical terms should not be used to classify spectroscopic gratings, we will give short remarks about these and other grating nomenclatures, which are often found in literature.

Grating types, named according to the used mounting, will be discussed in Section 3.

2.1 Surface-corrugated gratings: blazed, sinusoidal, and lamellar profiles

The grating profile determines the wavelength-dependent diffraction efficiency. So it is necessary to theoretically identify the optimum profile for each application and to master the fabrication technology to experimentally implement this profile as accurately as possible. The most important profile types are shown in Figure 3.

Gratings with blazed profiles are interchangeably called *echelette* or *sawtooth* gratings; in Japanese literature, this profile type is also called *serrated* gratings. Gratings with lamellar profiles are interchangeably called *binary* gratings.

The blazed grating profile is the most important type as it often allows to achieve the highest diffraction

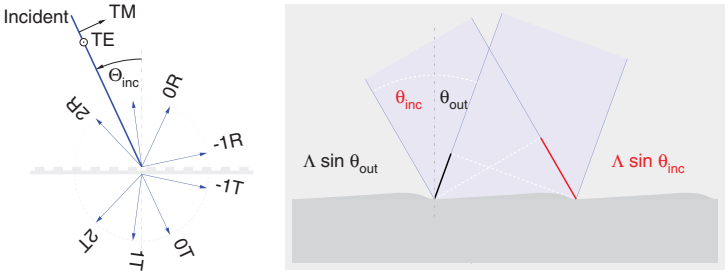

Figure 2 Polarization and diffraction order numbering (*left*). Phase differences for incident and diffracted beam (*right*).

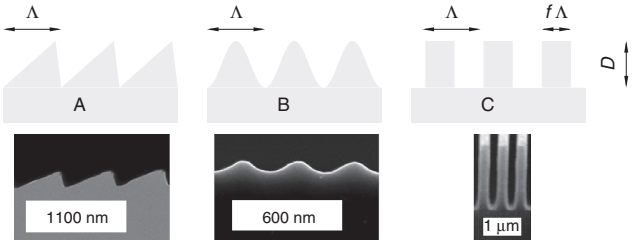

Figure 3 Types of surface-corrugated grating profiles: blazed (A), sinusoidal (B), and lamellar surface profile (C). Each of grating period Λ and grating depth *D*. Lamellar profile with a filling factor *f* (*top*). Scanning electron microscope (SEM) pictures of corresponding grating types (*bottom*).

efficiencies for a specified wavelength region. The smaller facet of the blaze profile is called antiblaze facet. To reach highest efficiencies, the specified blaze and antiblaze angles known from theoretical optimization have to be approached by carefully complying with the correct resist development strategy. Some theoretical investigations concerning optimal blaze and antiblaze angles can be found in [6].

A *blaze* profile recorded by IFL will show slightly rounded edges and an antiblaze slope, which is smaller than 90° as discussed in Section 6. Typically, these gratings have maximum resist heights between 90 nm and 120 nm. Reactive ion beam etching of IFL recorded resist structures into fused silica or other materials allows to achieve blaze depths of more than 1 µm, which yields highest diffraction efficiencies in the near-infrared spectral region if used in reflection. For extreme ultraviolet (EUV) applications, blaze depths below 50 nm are possible.

For *sinusoidal* profiles, a rigorous numerical optimization often shows that deviations from an ideal sine profile allow higher efficiencies. If these deviations are exactly known from rigorous calculation, they can be realized with an adapted resist technology by carefully choosing the development parameters. An IFL recorded sinusoidal interference pattern can thus be transformed into a sinusoidal-*like* surface pattern.

2.2 Surface corrugated vs. volume holographic gratings (VHG)

Different types of *surface-corrugated* gratings were already introduced. If made by IFL (see Section 4), these surface-corrugated gratings are often called *holographic gratings*. Confusingly, *volume holographic gratings* (VHG) are yet another grating type. VHG and *volume phase gratings* denote the same.

To manufacture VHGs, a 3- to 100-µm-thick layer of photosensitive material is used, typically sandwiched between protecting substrate materials. The entire volume of this photosensitive layer is exposed by a laser interference pattern, changing the refraction index. Some materials show a strong surface corrugation, additionally to the intended index variation *inside* the photosensitive volume layer (see, e.g., [7]). Typically, these materials are not used for high-end spectroscopic gratings.

Both surface-corrugated and volume holographic gratings can be used in transmission or in reflection mode. Both grating types theoretically allow to achieve diffraction efficiencies close to 100%. In reality, efficiencies above 90% are reached for both types. Both types can be fabricated showing very low scattering.

Thermal expansion as well as material imperfections (stress birefringence, bubbles and inclusions, inhomogeneity, and striae) will impair the entire volume holographic grating performance including effects from both protecting sandwich substrates. High-end spectroscopic surface-corrugated gratings working in reflection, on the other hand, do not suffer from material imperfection of their substrates. Nevertheless, these gratings follow the thermal expansion of their substrate material.

Transmission VHGs also show reflected diffraction orders. Spectrometers using VHGs, thus, may suffer from very special specular ghost paths, as discussed in [8].

2.3 Miniaturized gratings, metallic substrates, chirped depths, grisms

To design compact handheld spectrometers, different approaches are used. To benefit from high resolution and throughput of a *miniaturized* Carl grating, the recording IFL setup also has to be modified. A recording concept based on the introduction of a supplementary hologram was introduced in Brunner et al. [9]; see also the miniature spectrometer in Figure 4 (*left*).

Metallic substrates are desired to build lightweight gratings, allowing fast rotations for quick measurements. These substrates not only benefit from a lightweight skeleton matrix structure but also allow to integrate pads for mechanical fixation. Figure 4 (*center*) shows a concave aberration corrected grating on a metal substrate and Figure 4 (*right*) a metal substrate plane grating with integrated pads for clamping. Typically, the gratings are replicated on metallic substrates. Of course, a photoresist profile can be transferred by dry etching, or the grating can be directly mechanically ruled into the metallic substrate or a specifically smooth metallic layer on top of the metallic substrate.

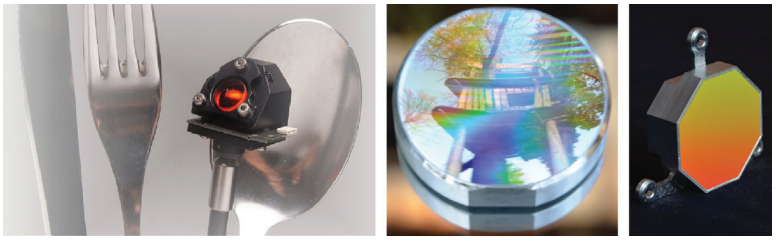

Figure 4 Miniature spectrometer, imaging concave aberration-corrected grating on metal base and plane grating on metal base.

A smart technique used for efficiency achromatization of blazed spectroscopic gratings is to chirp the profile depth (see Figure 5). Hence, specific regions on the grating are depth optimized to reach the highest diffraction efficiencies for specific wavelengths. The fabrication of Carl gratings with a clean and continuous transition region between different profile depths is shown in [10, 11].

The composition of a grating and a prism is called a *grism* (see [12]). It is applied to in-line presentation of the spectrum often desired in space spectrometers, to special femtosecond pulse-shaping designs, and it is an enabling technology for reduced volume immersed grisms and many other applications. For a grism in KRS5, see Figure 6. KRS5 is the short name for thallium bromoiodide, a high-index infrared transparent crystal material.

Most spectroscopic gratings are one dimensional. However, there are applications as antireflection coatings (see below), polarization couplers, photonic crystals, and others, where two-dimensional gratings are used. Figure 6 (*left*) shows a two-dimensional grating made by IFL.

2.4 Grating types according to application

This paper will mainly focus on gratings for spectroscopy. However, there are numerous other applications where gratings are used. Two grating types having advantages when used in combination with spectroscopic gratings shall be discussed in more detail.

So-called *moth eye gratings* are subwavelength two-dimensional gratings, which act as broadband antireflective structures for a wide range of angles of incidence – they are a successful mimicry of nature [13]. As the grating period of these structures is smaller than the wavelength of the used light, and thus, all diffraction orders are evanescent, they can be subsumed under subwavelength

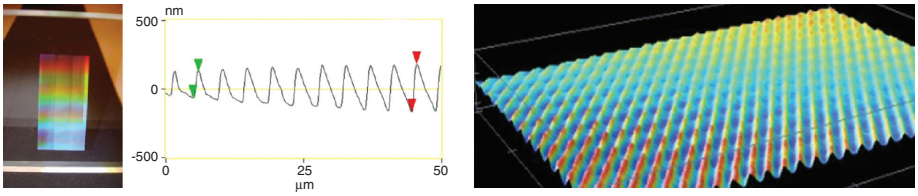

Figure 5 Photography, AFM of the transition region with chirped depth and microscope image of a blazed grating with different profile depths fabricated as monolithic grating.

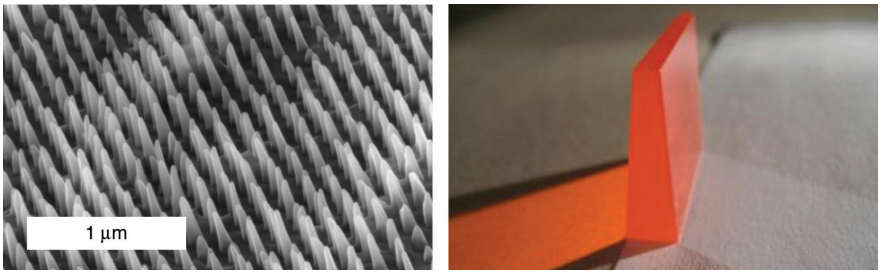

Figure 6 Two-dimensional grating written with IFL (*left*), and grism in KRS5 material (*right*).

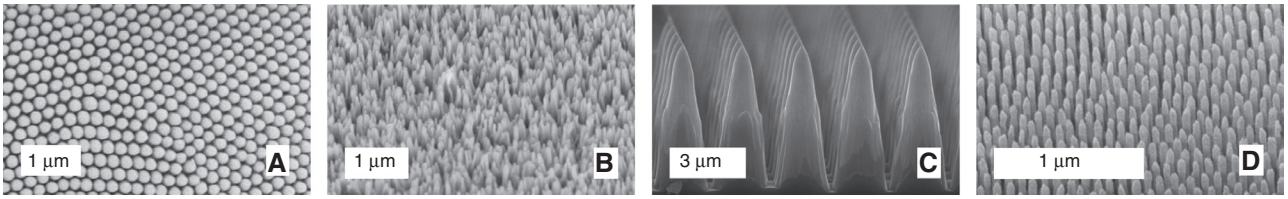

Figure 7 REM pictures of a moth eye (A), and moth eye-like structures, realized with different technologies: replicated into polymer with preceding plasma etching into SiO_2 (B), e-beam lithography into silicon (C), and micelle lithography into SiO_2 (D).

gratings (SWG) or zero-order gratings (ZOG). Fraunhofer already observed in 1817 that glass plates with a chemically affected surface show a lower reflection but not a reduced transmission [14], what seems to be contradictory to their matt surface. In contrast to antireflective coatings using interference effects from the interfaces of one or many different coating layers, moth eyes reduce the amount of reflected light by introducing a continuous transition of the refractive index from air to, e.g., glass and, thus, prevent Fresnel losses from the very beginning. This smooth refractive index transition acts as a graded refractive index structure (GRIN). Already, Taylor [15] patented the technology to etch glass surfaces to enhance transmission. Also, Smakula worked on this topic before inventing his famous T-coating at Carl Zeiss Jena [16]. Again, it took a longer technological development until Minot [17] successfully used chemical etching to achieve a broadband antireflective coating. Nowadays, different technologies are used for the commercial production of these subwavelength structures. Either stochastic surface structures are fabricated by maskless plasma etching or more or less periodic structures can be written with IFL or e-beam lithography, or self-organized surface layers are used as a mask for structuring (e.g., Morhard et al. [18]) (see Figure 7).

Plasma-etched stochastic structures (e.g., Schulze et al. [19]) provide antireflective properties for a broad wavelength range and a wide range of angles of incidence without strong ghosts. Using IFL, moth eye structures can be written on different surface shapes as concave or freeform optical surfaces and even on top of diffraction gratings or on top of microlens arrays (see Figure 6, *left*). Additionally, these complex microstructures can be dry etched into many different materials, e.g., silicon [20], reducing the Fresnel loss of about 30% from each side of a silicon wafer for a high-temperature sensor application. These moth eye gratings are of fundamental importance, as they can be used in many optical devices as, e.g., with lenses needed for microscopy, photography, semiconductor illumination, and many others. These subwavelength grating structures can be commercially replicated (see, ORAFOL, Fresnel Optics GmbH [21]), e.g., for display production or in brightness-enhancing films (BEF).

The term *hybrid optics* stands for the combination of refractive and *diffractive* surfaces in one optical device. As the sophisticated fabrication technology for *diffractive optical elements* (DOEs) used in hybrid objectives is quite similar to that of concave aberration-corrected gratings, these elements shall be at least mentioned here. A more detailed discussion can be found in Brunner and Dobschal [22]. The use of diffractive surfaces in system design typically allows a superior optical performance while minimizing system size. The bottom picture in Figure 8 shows an example of a very compact hybrid objective design.

Here, the number of optical elements and, thus, size and weight could be drastically reduced without loss of performance by using two diffractive surfaces in the objective design. The lenses with a diffractive surface are shown in gray color in Figure 8 (*bottom*). Also, the working distance of objectives using hybrid lenses can be increased by a huge factor compared to classical optics designs (see [23]). Other commercial solutions are available for photography (see, e.g., a discussion in Brunner [24]).

2.5 Thin vs. thick gratings

The terms *thin* and *thick* should not be used to classify spectroscopic gratings.

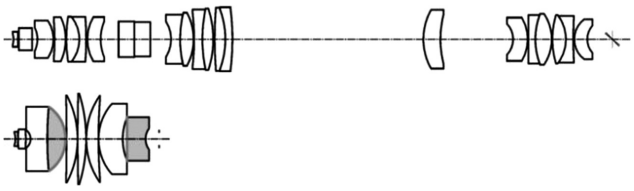

Figure 8 Size comparison of refractive (*top*) and hybrid optical design concept (*bottom*) for a LASIK objective with *equal optical performance*.

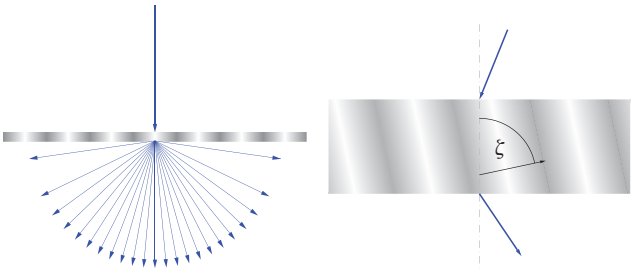

Figure 9 Typical diffraction regime for a thin (*left*) and a thick volume holographic grating (*right*). The angle ζ between surface normal and grating vector is called slant angle.

However, historically, these terms are used to distinguish between *thin* gratings following the Raman-Nath regime [25] with many diffraction orders ($\Lambda \gg \lambda$) and *thick* or *volume holographic gratings* (VHG) following the Bragg regime [26] with often only one diffraction order ($\Lambda \approx \lambda$) (see Figure 9). The terms *thin* and *thick* are not directly related to the grating depth but mark their selectivity of wavelength and angle – an analytical criterion to distinguish thin from thick gratings is already given in [27]. Gratings with neither Raman-Nath nor Bragg behavior are sometimes called *high-frequency* ($\lambda/\Lambda \sim 4 \ldots 100$) or *intermediate* gratings ($\lambda/\Lambda \sim 1 \ldots 10$).

The reason for still using the above nomenclature results from the desire to analytically describe the diffraction behavior. It is possible from Raman-Nath theory to predict diffraction efficiencies into all diffracted orders for thin gratings with a sinusoidal refractive index modulation. The Kogelnik theory allows to predict wavelength- and angle-dependent diffraction efficiencies for the first diffracted order of thick VHGs with sinusoidal refractive index modulations. Additionally, there are numerous publications concerning analytical prediction of diffraction efficiency for intermediate and high-frequency gratings (see, e.g., Golub and Friesem [28]). In most cases, these analytically calculated results slightly differ from the rigorously numerically calculated results (experimental results should be identical to rigorous). Nevertheless, these analytical approximations allow to better understand the physics behind the diffraction phenomena and always give at least a good starting design for a rigorous optimization.

The term Bragg grating is used for all transmission gratings with $\theta_{inc} = \theta_{out}$ (autocollimation for one reflected diffraction order). This geometry provides an efficient coupling of diffracted waves and, thus, very high achievable diffraction efficiencies. If the grating is used in reflection instead of transmission it is called Littrow mount (see Figure 10).

2.6 Transmission vs. reflection gratings

Reflection gratings for spectrometers are most often metal coated. Typically, this metallic coating has a thickness, which prevents light to be transmitted. Gratings with reflection efficiencies close to 100% used with high-energy laser beams are mainly realized using dielectric multilayer mirrors (see Rumpel et al. [29]).

On the other hand, *transmission* gratings are designed to ensure a high diffraction efficiency in transmission. Nevertheless, also in transmission gratings, reflected diffraction orders with non-negligible efficiency will occur. The number of effective diffraction orders is derived from the grating equation. At least concerning stray light in a spectrometer, this is a disadvantage of transmission gratings.

2.7 Classical vs. conical diffraction

The incident light and the surface normal of a one-dimensional grating define the plane of incidence. If this plane of incidence is perpendicular to the groove direction ($\Phi = 0°$),

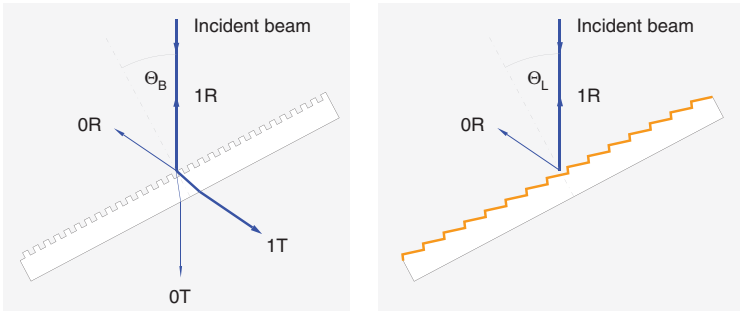

Figure 10 Gratings mounted in autocollimation are called Bragg gratings if used in transmission (*left*) and Littrow gratings if used in reflection (*right*) – the reflective top coating is emphasized in gold color.

diffracted light completely propagates in that plane. This geometry is called *classical diffraction*. However, if this plane of incidence is inclined to the groove direction, then all diffraction orders form a cone; thus, the diffraction is called *conical diffraction*. These cones are visualized in Figure 11 for azimuthal angles of Φ=1°, 65°, and 90°.

Not all software packages mentioned below allow to calculate conical diffraction problems.

2.8 Phase vs. amplitude gratings

If diffraction effects are determined only by phase changes applied to the incident light beam, the term *phase gratings* is used. Phase gratings are written, e.g., into photoresist, etched into fused silica or copied with epoxy or acrylate on any transparent substrate. Metallic spectroscopic reflection gratings are also phase gratings!

Transmissive zones arranged in an opaque mask are called *amplitude gratings*, as, e.g., grating structures, photolithographically written into masks covered with a chromium layer. The total transmission of all transmitted diffraction orders will typically not exceed the ratio of 'open' to metal area – the interesting exception of enhanced transmission through subwavelength apertures (see, e.g., Weiner [30]), and all related controverse discussions shall not be detailed here (see, e.g., Glaser [31] and literature cited there).

As this nomenclature is sometimes confusing, it should not be used to classify spectroscopic gratings.

3 Grating mounts

Several optical designs are possible to image the light in a spectrometer from the slit to the detector.

Spectroscopic diffraction gratings are either *plane* when used, e.g., in Czerny-Turner mounts or *curved* when used in a flatfield, Offner or Rowland spectrometer (see Figures 12 and 13). Curved typically means concave or convex spherical, but also aspherical and *freeform* grating substrates can be used for design optimization.

For a plane grating, additional imaging optics are needed. A concave grating typically will be the only optical element in the entire spectrometer.

One of these different *mounting* options in a spectrometer is chosen to satisfy the demand for highest resolution, throughput, and signal-to-noise ratio (SNR) considering specified wavelength and dispersion ranges. Also, weight, miniaturization, temperature range, and vibration aspects may dominate the specification sheet. The throughput of a spectrometer measures the photon flux (energy/time) that passes the spectrometer from the source to the detector.

High resolution requires excellent focal properties. High throughput demands a large numerical aperture, identical to a low *F*-number (*F#*). Unfortunately, with increasing numerical aperture, the focal properties and, thus, resolution and SNR are reduced.

Using a convex Carl grating in an Offner mount allows a better resolution and a wider field, as needed, e.g., for hyperspectral applications. Though Dyson [32], Offner [33], Mertz [34], and others proposed very specific concentric design ideas, which even make very high numerical

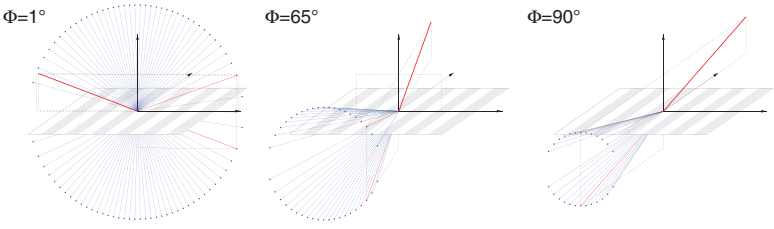

Figure 11 Conical diffraction geometry. Incident, specular reflected, and specular transmitted beam are highlighted with red color.

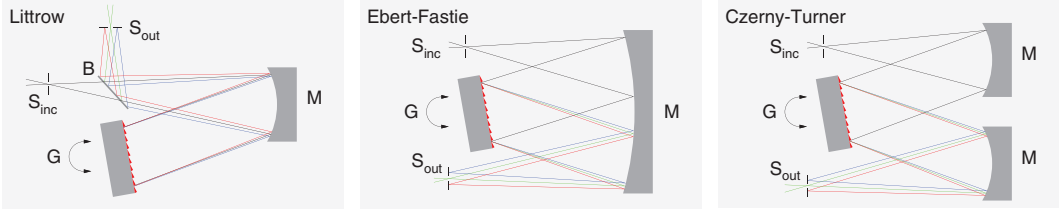

Figure 12 Plane grating mounts: Littrow (1862), Ebert-Fastie (1889/1952), and Czerny-Turner monochromator mount (1930). Gratings (G), mirrors (M), slits (S), and beamsplitter (B) are identified by their initials.

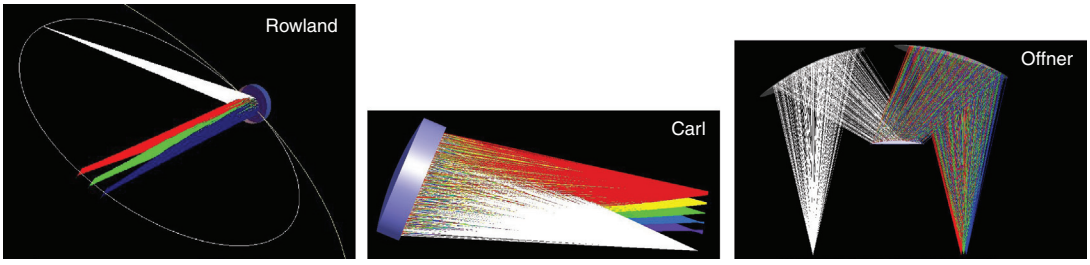

Figure 13 Concave and convex grating mounts: Rowland (1881)/Runge-Paschen (1902), flatfield or Carl (~1970), and Offner polychromator mount (1971).

apertures possible, an Offner grating can be optimized, manufactured, and thus treated as a Carl grating. The numerical optimization procedure of *convex* Carl gratings in an Offner mount is similar to *concave* Carl gratings in a flatfield mount – however, additional surfaces give additional design optimization freedom. From a technological point of view, there is no difference either: convex gratings can be mastered as concave gratings and copied later on.

For the optimization of Carl gratings and flatfield spectrometer design, expert knowledge in optical design, in IFL master fabrication, and in replication and coating of concave gratings are necessary. In some cases, a low-cost plane grating may be a favorable first guess for a simple design. However, for volume production of flatfield spectrometer devices, typically, the use of Carl gratings is the superior choice.

Plane grating mounts are shortly introduced. Following, for historical reasons, some aspects of Rowland gratings shall be compiled. After that, an introduction to Carl gratings is given.

3.1 Plane grating mounts

For many decades, only mechanically ruled gratings on *plane* substrates were available. A plane grating needs a pair of telescopes for viewing the spectrum – when used, e.g., in a Czerny-Turner or Ebert-Fasty mount as shown in Figure 12. One telescope collimates the light from the source onto the grating and the other images the diffracted light to the detector. Of course these 'telescopes' can be realized by any optical element from a spherical or paraboloid mirror, even a simple lens in the visible spectrum or an optimized objective or even a catadioptric system.

For all spectrometers, beginning from the 19th century up to now, mechanical rigidity and thermal stability have been of utmost importance. Littrow [35] proposed to use autocollimation for prism spectrometers. This design required only one telescope instead of two and, thus, allowed a much easier, compact, and more stable arrangement (see Figure 12).

The Czerny-Turner design principle shown in Figure 12 is called the 'W' configuration. To alleviate stray light, there is a crossed beam version of the Czerny-Turner mounting and other configurations. A discussion of pros and cons concerning different aberrations, stray light, and costs can be found, e.g., in Davis [36] and literature cited there. Until 1881, all spectrometers used plane gratings.

3.2 Rowland grating mounts

It was a milestone for spectroscopy when Rowland [37] combined focusing and grating dispersion properties in one single element: the *concave grating*. Additionally, absorption in the UV region could be avoided, as there was no glass anymore in the optical path of light.

Grooves for a Rowland grating have to be straight and equidistant in a projected tangential plane. Rowland explicitly states that the grooves are NOT equal on the arc of the circle – 'I do not rule them in this manner, but the spaces are equal along the chord of the arc!' [38]. The necessity of constant distance on the secant of the spherical grating substrate easily allows IFL but has to be kept in mind with mechanical ruling.

A circle with the diameter of the grating radius is called the Rowland circle. Providing experiments and corresponding mathematical basics, Rowland proved, if a source is placed on the Rowland circle, the entire diffracted spectrum will be brought to a meridional focus on the same circle. Astigmatism provides that a pointsource will be imaged into a vertical line; see Runge-Paschen mount in Figure 13 [39].

Numerous mountings were proposed, as, e.g., for collimated incident light on astronomical spectroscopes from Wadsworth in 1894, a Littrow-like mounting from Eagle in 1910, an optimal angular separation of 70.25° for minimal

image degradation from Seya and Namioka in 1952. The Seya-Namioka mount was mainly used for vacuum UV wavelength region below 180 nm, where additional absorption losses of aluminum mirrors made plane grating mounts disadvantageous. However, starting already in 1959, improved coating technology allowed to use Czerny-Turner mounts as well. The reduced aberration of Czerny-Turner mounts, with near stigmatic imaging, provided an advantage in overall performance over a Seya-Namioka mount. (A wavefront is described as stigmatic if it has no aberrations.) None of these mountings shall be presented graphically nor further discussed because there is plenty of literature on these and other mountings, and with the invention of Carl gratings in the 1970s, all of the designs mentioned above became more and more obsolete (see Labeyrie and Flamand [40]).

3.3 Carl grating mounts

It was shown that concave gratings allow the combination of focusing and dispersion in one element. After the invention of the laser around 1960, gratings made by IFL outperformed mechanically ruled gratings, but only in a few aspects. At this time, IFL-exposed diffraction gratings showed equidistant grooves – just as mechanically ruled did. Until the 1970s, spectrometers were restricted to the throughput and resolution limitations caused by the inherent astigmatism and coma aberrations of any of the above-mentioned mountings. These limitations were independent from the manufacturing technology – mechanical ruling or IFL using plane waves.

Already, Rowland thought about optimizing performance with non-equidistant grooves. But only with the boom of IFL during the 1970s did it turn out that using spherical instead of plane waves offers new degrees of freedom to reduce aberrations for all of the known conventional mountings. These Carl gratings have nonuniform spacings and curved grooves. Designs with three instead of only two stigmatic points based on analytical functions were identified (see Güther and Polze [41]). Subsequently, these analytical designs were used as an initial choice for further numerical optimization to reduce astigmatism and coma and, finally, even to correct defocus for flat-field gratings. Even Schmidt plates [42] or other aspheric predeformation of the interfering wavefronts can be used to enhance performance. An excellent overview of many of these designs is given in [3]. Though aspheric and toroidal grating substrates were used already before IFL exposure, they may contribute to even further reduction of aberrations for IFL exposed gratings.

Today, the best final design is obtained through numerical optimization from scratch (see Bittner [43]). Substrate radius, entrance slit position, and the detector position do not have to meet any fixed relationship. The resulting concave aberration-corrected grating can only be made by IFL and cannot be mechanically ruled. For these gratings, the acronym of a Carl grating was introduced, as this technology provided the next milestone for applications of diffraction gratings in spectroscopy. *Throughput and spectral resolution* were significantly improved.

Nevertheless, expert knowledge, both for theoretical design as for manufacturing is as advantageous as a mutual understanding and tight cooperation between the designer and the manufacturer to always keep in mind coherent and incoherent reflection management, tolerances, and other pitfalls.

For high-end spectroscopic gratings, thus, a Carl grating is the best choice. Highest diffraction efficiencies identical to plane gratings will be achieved using blazed grating profiles as discussed in the next chapter. Measured data is presented in Figure 25. The often commented low diffraction efficiency of these designs (e.g., Loewen and Popov [5]) cannot be confirmed.

3.4 Monochromator vs. polychromator mounts

The terms monochromator or (flatfield) polychromator mount are determined by the application of the spectrometer device. A *monochromator* uses one entrance slit and one exit slit, both fixed. The grating is rotated to select the wavelength. In a *polychromator* device, all components are fixed: the entrance slit, the grating, and the detector.

As IFL allowed to realize Carl gratings with aberration minimization for the entire spectrum in a plane focus region, flatfield polychromator, and also monochromator designs using Carl gratings are advantageously in common use. Plane area detectors, as, e.g., CCD or CMOS detectors can be used.

In the near future, one might go back to a bended focus region – as it was already done decades ago with deformed photographic plates and films. Bendable CCD electronics can, nowadays, use this additional degree of freedom again to even further enhance resolution and throughput.

4 Fabrication technology

Spectroscopic diffraction master gratings are typically fabricated using *IFL* or *mechanical ruling*.

For high-end spectroscopic diffraction gratings, IFL written Carl gratings are superior to mechanically ruled gratings. They typically show

- **less scattering**: while mechanical ruling suffers from statistical groove position errors, an interference pattern does not,
- **no ghosts**: while mechanical ruling suffers from tiny periodical groove position errors, an interference pattern does not, and
- better **corrected astigmatism and coma**: the design optimization merit function for Carl gratings allows to minimize these aberrations (see Bittner [43]).

They can be illuminated on steep aspheric substrates, which are nearly impossible to rule conventionally, and typically, a wider choice of groove spacings and a wider choice of grating sizes are available.

Figure 14 shows the orientation of the sinusoidal fringe system during IFL exposure yielding sawtooth-shaped surface-corrugated grooves after development.

For large quantities, IFL written and mechanically ruled master gratings are replicated.

As Carl gratings are made by IFL, few comments on historical terming shall be given. Other lithographic technologies will be shortly cited.

4.1 History and terming of IFL

The idea to photograph the interference region of light was already mentioned in 1868 by Zenker. Wiener [44] showed how to expose a photoresist with standing electromagnetic waves. In these years, fascinating investigations were followed by Lippmann, Cotton, Lyman, Cornu, and many others. Finally, Michelson [45] points out in 1915 that this interference photography using a mercury lamp should make it possible to manufacture a spectroscopic grating with a resolution exceeding one million. The resulting interference pattern from two coherent plane waves depending on propagation direction is shown in Figure 15.

Ritschl and Polze [46] demonstrated in 1958 a resolution of 4000 l/mm in a photographic plate – photographic plates were not known before to provide such high resolution at all. However, due to the low available power using lines of a mercury lamp, this technology did not permit very large gratings.

It was the invention of the laser that finally allowed the breakthrough of IFL.

While Ritschl correctly terms 'photographic recording of interference fringes', it got more and more common to use the term 'holography' interchangeably with IFL in the manufacturing of Carl gratings in the 1970s. Thus, until today, these gratings are often called 'holographic gratings' instead of interference lithographically made gratings.

4.2 Interference lithography (IFL)

IFL is a standard technique to fabricate high-end spectroscopic gratings. The entire technology chain includes exposure, resist development, etching when indicated, and replication if desired.

Exposure from one substrate side produces sinusoidal profiles, counter-propagating waves allow blazed surface profiles. Point sources instead of plane waves allow for additional aberration correction. All technologies may be applied for plane and concave or other freeform substrates. Carl gratings are favorably exposed with two counterpropagating spherical waves. Figure 16 shows an overview to different IFL technologies.

Microroughness, flatness, parallelism, and material homogeneity of the used *substrates* are crucial for successful manufacturing of gratings with high efficiency and low scattered light. The exact parameters depend on substrate

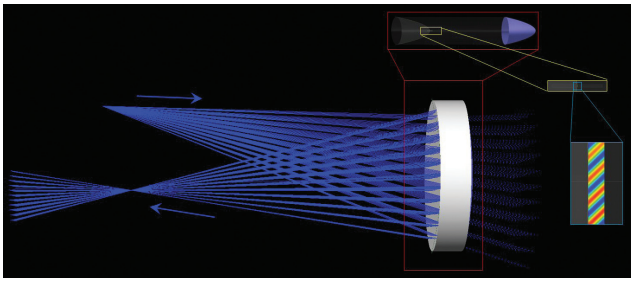

Figure 14 Exposure setup for a Carl grating. Substrate is zoomed anamorphicly by a factor of 20, and concave front surface is zoomed again to show energy distribution in 100-nm-thick photoresist region near vertex.

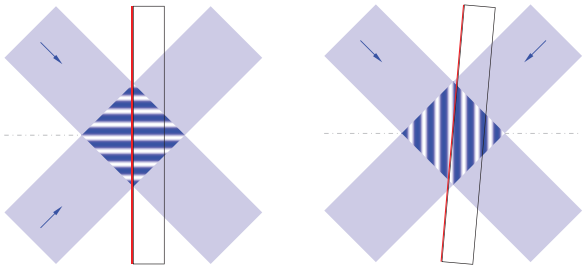

Figure 15 Sinusoidal interference pattern depending on propagation direction from two coherent plane waves. The resist layer on top of the substrates is highlighted in red color.

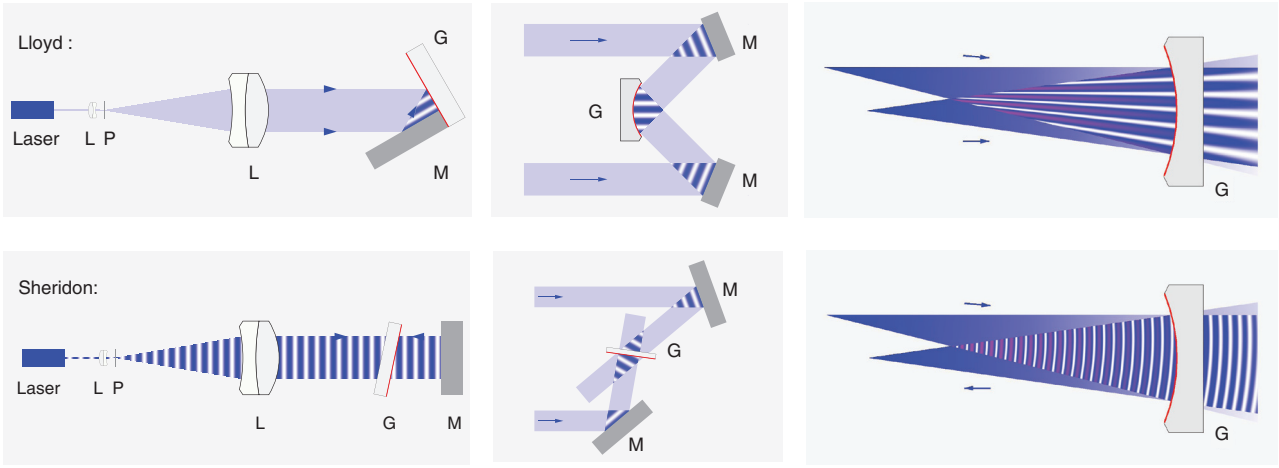

Figure 16 Different IFL setups for the exposure of plane and Carl gratings. The sinusoidal interference pattern from two coherent waves allows to generate symmetric profiles (*setups in the top row*) and blazed profiles (*setups in the bottom row*). Further correction is achieved using point sources (*right*) instead of plane waves (*left, center*). Grating substrates (G), lenses (L), mirrors (M), and pinholes (P) are identified by their initials. Refraction inside optical elements is not accounted for.

shape, illumination technique, and the customer specification sheet. As an example, Nagata and Kishi [47] used glass blanks polished to a flatness of $\lambda/5$ and a parallelism of a few seconds of arc.

Exposing a resist coated substrate with a stationary interference fringe system yields a latent structure with modulated solubility. A temporal snapshot of the field amplitude distribution is shown in Figure 17. With ongoing time, the white points of zero amplitude are stable in horizontal position. However, in vertical direction, the field distribution is flowing downward, and thus, the energy distribution already shown in Figure 15 results. The latent resist structure, which results from exposure, is transformed into a surface-corrugated profile during the subsequent resist development process. The exposure using plane waves produces a *sinusoidal pattern*. Resist thicknesses from below 100 nm to much more than 400 nm can be used depending on the desired grating profile design.

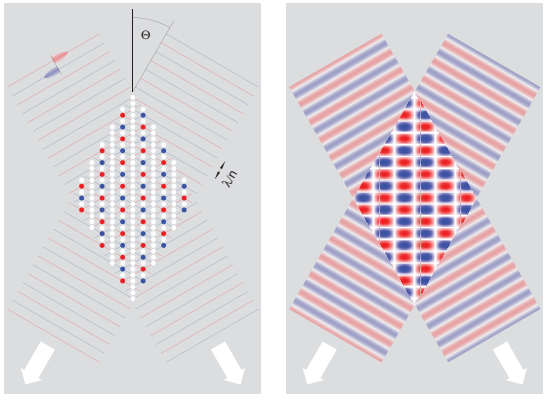

Figure 17 Snapshot of TE-polarized electrical field amplitude. Colors indicate min and max (red and blue) and zero points (white). For clarification only, min and max are shown in left picture. Position of zero points is stable over time, temporal average of field amplitudes results in sinusoidal energy distribution with $\Lambda=\lambda/(2n\sin\theta)$.

For *plane substrates*, the exposure of grooves with a *blaze contour* after development is well-known since Sheridon [48] showed how to incline the photosensitive layer to the nodal planes of the interference wave field (see Figure 15 (*right*) and Figure 16). This setup needs a longer temporal coherence length, which implies coherent interaction of unwanted reflections. Thus, pros and cons have to be kept in mind when choosing a specific IFL setup.

Carl gratings on *concave or convex substrates* are exposed using spherical or aspherical wavefronts. To achieve a blazed groove contour after development, Güther and Polze [41] proposed for exposure of Carl gratings to use the interference fringe system of a converging spherical wave through the back of the blank and a diverging source in front of the blank. Sometimes, diverging and converging waves are entitled as real and virtual source types.

Further technologies are used to achieve blazed grooves, such as sloped dry etching (see Flamand et al. [49]) and rarely also the elaborated Fourier synthetic method (see Breidne et al. [50]). The last-named method allows to achieve larger grating depths.

Using IFL with point sources also allows the exposure of a focusing grating on a *plane* substrate.

If blaze-wavelengths other than 190–250 nm are required, the depth of the blazed resist surface profile can be *diminished* for EUV use or *enhanced* for IR use with reactive ion beam etching (RIBE) (see Fechner et al. [51]). In Figure 18, an etched blaze profile for NIR application is shown, which was enhanced by a factor of about 8.

4.3 Mechanical ruling

Mechanical ruling engines have been constructed during the last centuries by highly skilled and ingenious technicians and scientists as Fraunhofer, Nobert, Rutherfurd, Rowland, Michelson, and others. The so-called Michelson engine from 1910 was refined a few times but is still running, following [5]. Obviously, it was neither much easier nor economically attractive to build a new machine nowadays. Further details about technological challenges and other aspects concerning mechanical ruling can be found in these sources, too.

Also, Zeiss, which started work on mechanical ruling engines in 1925, and restarted building these ruling machines after World War II, both in Jena and in Oberkochen, is still running two machines at the Jena location – though IFL is well established since the 1980s for manufacturing of Carl and plane gratings. The newest mechanical ruling engine is the so-called 'number IV,' which was built in 1976. For details on the history of mechanical ruling at Zeiss, see Kröplin [52].

The fringes of the interference pattern from spherical wavefronts form a set of hyperboloids or ellipsoids depending on the divergence or convergence of the sources. The exact reproduction of these patterns is crucial for aberration correction. Additionally, the desired facet angle on curved substrates varies continuously. For ruled gratings, in contrast, the facets typically are all in parallel. Modern ultra precision CNC machines theoretically allow to continuously reset the diamond angle without interrupting the ruling process what enlarged the scattering level of the grating in the past. However, it is not known to the author, whether a curved ruling with non-equidistant grooves on a strongly curved substrate combined with a diamond angle alignment has ever been successfully accomplished.

Though already Rowland constructed a mechanical ruling engine, which was able to rule on concave substrates, it is not possible to mechanically rule concave aberration-corrected gratings on these machines – so it is legitimated that the acronym Carl grating already implies the manufacturing by IFL.

4.4 Direct writing laser lithography vs. e-beam and other lithographies

IFL, as described above, uses the energy distribution in the interference region between two laser beams, which may have diameters between 10 and 1000 mm to expose a resist. This allows to expose areas of 100×100 mm^2 within a few seconds on arbitrarily curved substrates. *Direct writing laser lithography* allows to write blazed profiles with periods much larger than 10 µm, but only on slightly curved substrates. *E-beam lithography* allows to write lamellar and blazed profiles, but only few e-beam machines are modified to write on curved substrates, as reported in [53]. Typically, e-beam machines write only on plane substrates.

Direct writing laser (DWL) lithography uses a highly focused laser beam to expose the resist in the focus of a micro-objective. An *xy* stage or an *rθ* stage allows to move the substrate during writing and, thus, allows to expose arbitrary dose distributions. In accordance to the corresponding regime of movement, linear or circle trajectories are especially smooth, but other dose distributions are possible as well. These machines are commercially available to write on planar and also on slightly curved substrates. Lamellar gratings with periods in the order of the wavelength are possible if one trajectory is used to write a single groove [7]. By composing many single trajectories

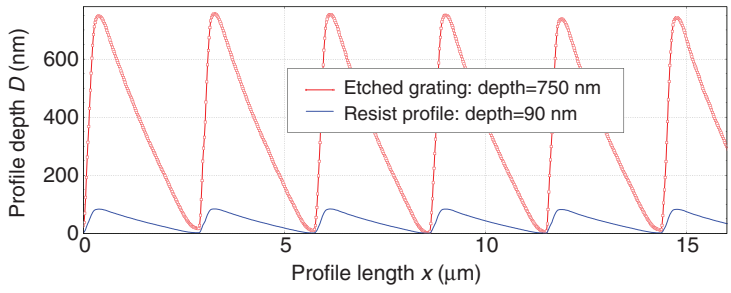

Figure 18 AFM of blazed profile before and after dry etching of a Carl grating on a concave substrate.

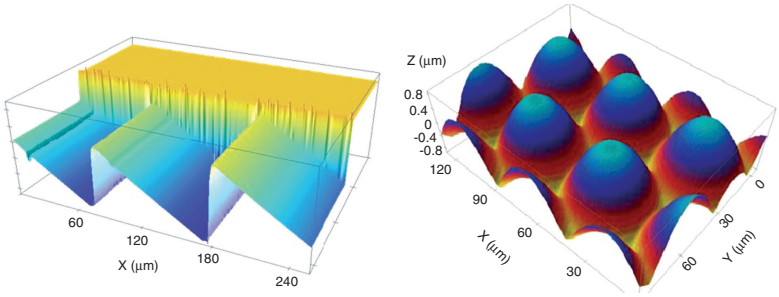

Figure 19 Diffraction grating with 10 l/mm (period Λ=100 µm), and depth of 4.3 µm (*left*), and microlens array (*right*).

into one substructure, nearly arbitrary height distributions can be written. To achieve a smooth surface, the period of these gray level structures has to be large compared to a single trajectory. Thus, blazed gratings with large periods, microlens arrays, and computer-generated holograms can be written (see Figure 19) (see Cumme and Deparnay [54]). The maximum height is restricted to the used resist thickness – typically between 100 nm and about 20 µm. Exposing an area of about 100×100 mm² will take a few hours depending on resolution.

There are *e-beam lithography* machines working in a similar writing regime as described above for DWL. Furthermore, there are e-beam machines using the much quicker regime of composing the desired dose distribution from rectangular patterns. The resolution is much higher compared to DWL, lamellar gratings with linewidth below 20 nm are possible. However, the writing time is still much higher compared to IFL. Gully-Santiago et al. [55] reports on e-beam-written silicon immersion gratings, but still mentions three key challenges: stiching effects causing ghosts, e-beam stage drift causing wavefront error, and write times of about 24 h making prototyping costly.

Semiconductor industry applies optical multiple pattern immersion lithography. Using a 193-nm wavelength ArF excimer laser, the image of a photomask is projected onto the wafer. In October 2014, Intel's Broadwell-based Core-M processor was sold using 14 nm technology – far below the once expected limit of resolution of $\lambda/2 \approx 100$ nm. This technology shall not be discussed here as the lenses that provide this quality are too expensive for producing small quantities of high-efficiency spectroscopic diffraction gratings. Additionally, spectroscopic gratings are extremely sensitive to stiching error-related ghosts, which occur from photomask alignment.

Wet-chemical etching of silicon yielding supersmooth surfaces, proximity lithography, Talbot lithography, contact copies, and other technologies are also promising for the manufacturing of special spectroscopic gratings.

5 Grating resolution and étendue

The *resolution R* to resolve two spectral lines with wavelengths λ and $(\lambda+\Delta\lambda)$ is

$$R=\frac{\lambda}{\Delta\lambda}=|m|\cdot N=|m|\cdot wG_{\#}$$

with m, the diffraction order number, N, the number of illuminated grooves, w, the total width of the grating, and $G_{\#}=1/\Lambda$, the number of lines per mm. To see the double yellow line of sodium $\frac{5893}{5896-5890}$, a resolution of about 1000 is needed. Typical values are given in Table 1.

High resolution can be achieved not only with a large illuminated grating area and a small period. Additionally, the used diffracted order and, thus, the mounting geometry are essential. For that reason, echelle gratings are used in orders m from 50 to 300 to achieve the highest resolution implying steep angles of incidence and diffraction.

A 20-mm-wide grating with 250 l/mm (R=5000) illuminated with light of 500 nm wavelength allows to resolve two lines with $\Delta\lambda$=0.1 nm.

Historically, resolution with prisms had been gradually increased to about 30 000 in the 19th century. Fraunhofer ruled 3601 grooves with a diamond directly into a glass surface with 0.44 Paris inch total length, i.e., 302 l/mm [56]. The American hobby astronomer

Table 1 Theoretical resolution limits for typical grating sizes and line numbers.

Grating size w	Line number $G_{\#}$	Diffr. order m	Resolution $\lambda/\Delta\lambda$
10 mm	50 l/mm	1	500
10 mm	500 l/mm	1	5000
25 mm	2000 l/mm	1	50 000
100 mm	5000 l/mm	1	500 000
100 mm	100 l/mm	150	1 500 000

Rutherfurd ruled 35 000 grooves with 690 l/mm in 1870. In 1873, the German watchmaker Nobert demonstrated with small microscopic resolution test plates that line densities of 8865 l/mm are feasible [57] – though 20 bands are not useful for spectroscopy. Rowland achieved a resolution of about 400 000, and in 1915, Michelson proposed that a resolution of 1 000 000 should be feasible if made by IFL as mentioned above.

Thus for the next decades, enhancement of resolution is not a topic anymore. Resolution for high-end spectrometers using Carl gratings often is limited by aberrations, tolerance management, or the used slit width – the number of illuminated grating grooves is not being a key restriction.

The *étendue* is a crucial parameter for spectrometers as for nearly any other optical instrument. The étendue G, also called beam parameter product (*in german*: Lichtleitwert), measures the amount of light, which can be fed through an optical system:

$$G = A \cdot \Omega,$$

where A is the area of any stop or pupil in the system, which receives radiation from a solid angle Ω. As the radiance of any light source, the power per étendue obeys the radiance conservation theorem and cannot be increased by any passive optical system (*in german*: 'Es gibt keinen Lichttrichter').

To achieve the highest SNR, any spectrometer designer is interested to maximize the étendue. But the width of the slit cannot be increased as this directly reduces the resolution. Unfortunately, increasing the slit height or the numerical aperture (solid angle Ω) also typically results in a reduced resolution and, thus, in radiance and SNR degradation. The best way is again a simultaneous numerical optimization of resolution and étendue.

6 Grating efficiency

The grating *efficiency* for metallic spectroscopic gratings is determined by the grating profile and, of course, by the quality of the metal [coating] layer.

To predict the *absolute diffraction efficiency* (aDE) of a certain grating profile and to compare it with measured values, these efficiencies have to be calculated as exactly as possible. First, some analytical and numerical calculation methods will be discussed. Catalogs often show *relative diffraction efficiencies* (rDE), which represent the ratio of the absolute diffraction efficiency to the reflection of a metallic mirror coated with the same metal coating layer. For general discussions, often the *perfect diffraction efficiency* (pDE) is investigated – i.e., the diffraction efficiency that results for the theoretical assumption of a perfectly conducting material (see *top* of Figure 20).

Qualitative differences between aDE, rDE, and pDE will be discussed in short as well as the influence of the measuring geometry and the influence of a thin aluminum

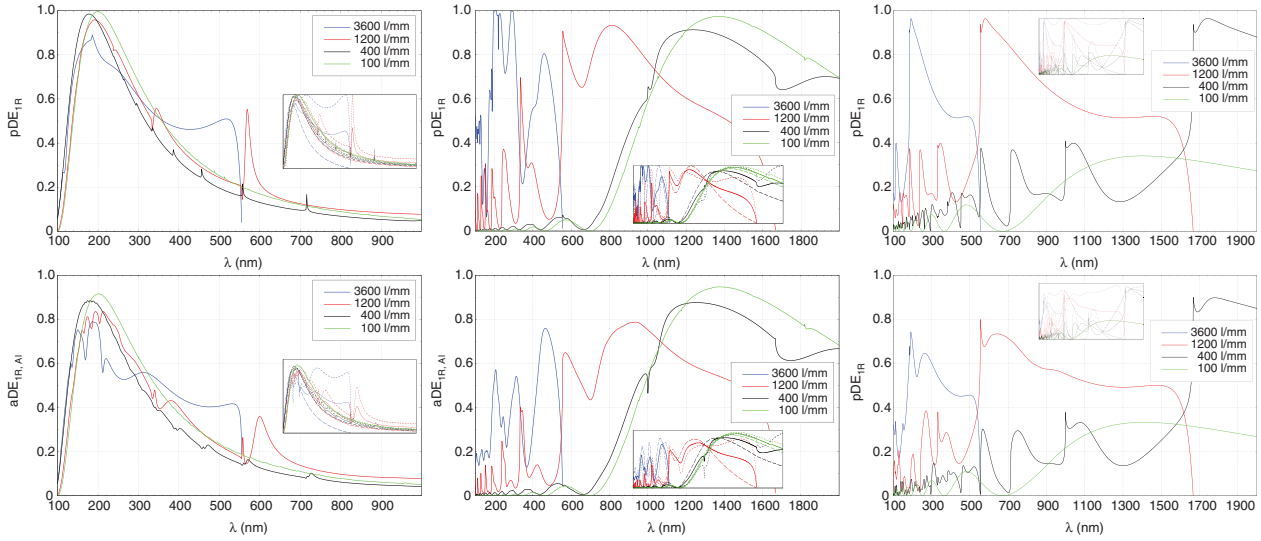

Figure 20 Perfect diffraction efficiency (pDE) for unpolarized light into the first reflected order (1R) on perfect conducting material (*top*) and absolute diffraction efficiency (aDE) for aluminum coated gratings (*bottom*) in autocollimation. Blaze profile with 100 nm depth (*left*), and 700 nm depth (*center*), and sinusoidal profile with D=0.3 Λ (*right*, exception: for 100 l/mm: D=410 nm). Insets: efficiencies for TE- and TM-polarized light are shown additional with dashed lines.

oxide layer, which is always on top of an aluminum coating without a capping layer of, e.g., MgF_2.

6.1 Numerical calculation methods

Diffraction behavior of gratings can be exactly calculated by solving the Maxwell equations including the appropriate descriptions of geometry and wavelength-dependent permittivity. Exact analytical solutions exist only in a few cases. However, there are many different so-called rigorous methods to solve the Maxwell equations numerically. Analytical approximations cannot be used to obtain the exact prediction of the diffraction efficiency for metallic gratings used in spectroscopy.

These rigorous methods include, e.g., integral methods, rigorous coupled wave analysis (RCWA), Fourier modal method (FMM), rigorous modal analysis (RMA), Chandezon method (C method), finite element methods (FEM), and many more. For a classification of these methods and details on the different electromagnetic theories to solve the Maxwell equations, the interested reader is referred to, e.g., Loewen and Popov [5] or Kleemann [58] to get an introduction. Each method has pros and cons, still after much more than 40 years of sublimation of both theory and computer code.

Optimizing a desired spectrometer performance requires a certain exactness while solving the correspondent grating design problem. As new software is not implemented overnight, many users will use commercially available code. They will decide between different software modules by CPU time consumption for reaching the desired level of exactness. Also user friendliness of the graphical user interface (GUI) is important, e.g., to include measured atomic force microscopy (AFM) profiles or to perform multiparameter analysis or optimization. The last but not the least costs have to be considered. Some well-known commercial solvers, e.g., include PCGrate [59] as an integral solver, unigit [60] implementing RCWA and C method, JCMwave [61], and WIAS-DiPoG [62] implementing FEM, VirtualLab [63] implementing FMM, and GSolver [64] implementing RCWA, and RMA. All the results shown here are calculated with IESMP or PCGrate [59]. IESMP is a proprietary software package of Carl Zeiss company (see, e.g., Kleemann et al. [65]).

6.2 Theoretical efficiency prediction

The simulations shown in Figure 20 reproduce some diffraction efficiencies over wavelength for typical reflection gratings used in spectroscopy for unpolarized light to facilitate the discussion of diverse influences. First, the theoretical values shall be shown assuming a perfect conducting material and ideal profiles for autocollimation mount. $\sin\theta_{inc}=\sin\theta_{out}=\sin\theta_{Littrow}=\lambda/(2\Lambda)$ – the first diffracted order disappears ($\theta_{out}=90°$) for $\lambda=2\Lambda$ as can be seen in Figure 20 for $\lambda=556$ nm for 3600 l/mm. The insets show the efficiencies for TE- and TM-polarized light.

Plenty of literature presents rigorously simulated diffraction efficiencies. A discussion of efficiencies near 100% for lamellar gratings can be found in [66]. Breidne and Maystre [67] present grating depth-to-period ratios, where the diffraction efficiency for one polarization achieves 100% for Littrow mount, for sinusoidal, lamellar, and blazed profiles.

This spectral behavior already changes when realistic metallic materials are considered, typically aluminum (Al) is used in UV and VIS, and gold (Au) for NIR spectral range (see Figure 21).

Hence, it is both necessary to theoretically identify the optimal profile for each application and to master the fabrication technology to realize this profile experimentally as close as possible. The designer knows from experience whether a *holoblaze* or a *sinusoidal*-like profile is better adapted to the specification sheet concerning the wavelength-dependent efficiency. Holoblaze means the blaze profile, which typically results from IFL exposure, which may have a bit more rounded corners than blazed profiles from mechanical ruling. Depending on groove number and blaze wavelength (respectively, groove depth), the realized profiles may differ slightly – which may have

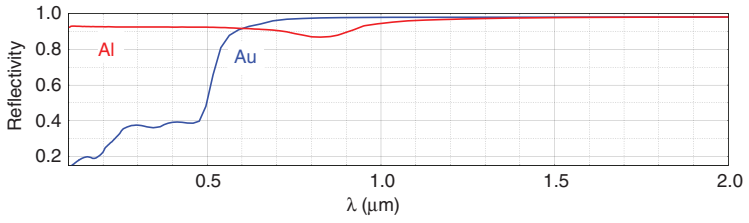

Figure 21 Reflectivity of aluminum and gold from [68].

significant influence on the wavelength-dependent efficiencies. As light sources and detectors are insensitive in the UV region, often blazed profiles with the highest efficiencies in the UV region, are desired.

As it is shown below, also the quality of the metal coating and the aluminum oxide depth on top may influence wavelength-dependent efficiencies – again depending on groove frequency and groove depth. Additionally, the mounting geometry, and if different, the measuring geometry may strongly influence the wavelength-dependent efficiencies.

6.3 Influence of refractive index

The possible influence of the *refractive index* shall be illustrated by the example of a 3600 l/mm Rowland grating used in the UV region (with an AFM-measured profile). For a wavelength of 193 nm (Palik [68]) presents a refractive index of n=0.11+i·2.22. The American Institute of Physics Handbook (AIP) presents n=0.12+i·2.07 [69]. Both values are shown as pink dots in the inset in Figure 22. The Palik value represents 92.6% reflection for normal incidence, the AIP value 91.4%. Our thermally evaporated Al layers show reflectivities of 86–89% – these reflectivities are represented in the colored region in Figure 22 inset.

The influence of the refractive index was investigated for complex values, all resulting in 87% reflectivity at 193 nm – see points *a*, *b*, *c*, and *d* in Figure 22 inset. To have a smooth transition the 'next' supporting wavelength was chosen to be 350 nm with a refractive index of (n=0.375+i·4.24), refractive index values in-between were linearly intrapolated. A significant shift of the resonance can be observed.

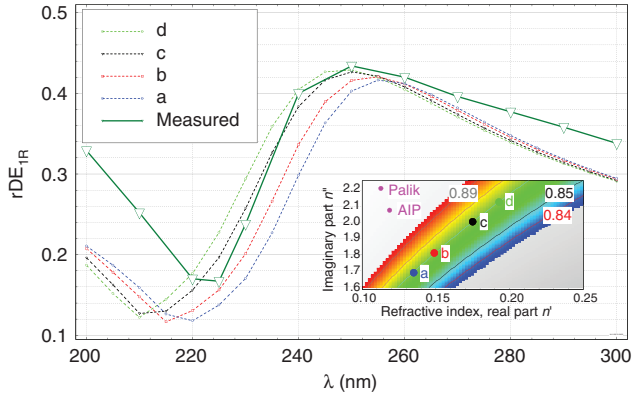

Figure 22 Diffraction efficiency of a 3600-l/mm grating for different refractive index assumed.

For this grating with 3600 l/mm, a thickness change of aluminum oxide at the surface from 0 to 6 nm has a similar resonance shifting influence as it was shown for the refractive index. As both the aluminum oxide layer on top, and the typically graded refractive index distribution near the surface of aluminum layers were investigated separately and ignored in this discussion here, no perfect match with measured data is expected.

6.4 Influence of replication

If replication technology is mastered well, there will be nearly no change in efficiency and scattered light level. Of course, there may occur a so-called 'generation problem': this describes the fact that only grating profiles of odd generations are similar to each other and to the master structure, and all profiles from even generations are similar to each other – according to the inverse surface corrugation profiles.

Using the example of a mechanically ruled 1200 l/mm plane grating with blaze profile, it shall be demonstrated that these small deviations in the blaze profile between even and odd replications will result in significant changes in diffraction efficiency. Figure 23 shows the measured diffraction efficiencies for a master grating and five subsequent replication tools. It can be clearly seen that all odd and all even generations group together.

Theoretically, this relationship is identical for Carl gratings. But as only concave gratings are used, the blaze profile for the concave generation has to be optimized – or for convex gratings, if Offner gratings are manufactured.

6.5 Influence of measuring configuration

For measuring the diffraction efficiency, not only the desired wavelength range and polarization have to be

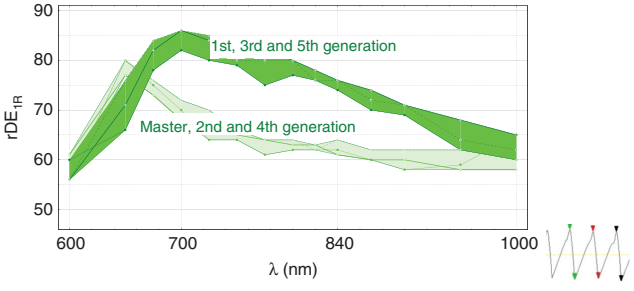

Figure 23 Measured diffraction efficiencies for a 1200-l/mm plane grating, which was replicated into 5th generation (*left*). Even generation AFM profile (*right*), odd generation AFM is just inverse.

specified but also the precise grating measuring geometry. If no angle of incidence is mentioned, often measured efficiencies into first order in autocollimation are expected.

Often grating efficiency over wavelength is measured in a monochromator configuration – with a constant angle of deviation γ. For practical reasons, this constant angle of deviation will not be zero, but, e.g., 5° or 30°. Nevertheless, sometimes for small constant angles of deviation, this monochromator mount is also called autocollimation, though $\gamma \neq 0°$. For these geometries, of course, the (wavelength dependent) angle of incidence is changed slightly, compared to autocollimation with $\gamma \neq 0°$. Writing the grating equation $\sin\theta_{inc}+\sin\theta_{out}=2\sin(\theta_{inc}+\theta_{out})/2\cdot\cos(\theta_{inc}-\theta_{out})/2=m\lambda/\Lambda$ with $\gamma=\theta_{inc}-\theta_{out}$ yields

$$\theta_{inc}=\gamma/2+\arcsin\frac{m\lambda}{2\Lambda\cos(\gamma/2)}.$$

If, now, the grating efficiency strongly depends on the angle of incidence, the diffraction efficiency for a certain wavelength also will change significantly.

Even if the constant angle of deviation into the first diffraction order is specified, only one (A) of four possible mount geometries is intended and should be used, as is demonstrated in Figure 24.

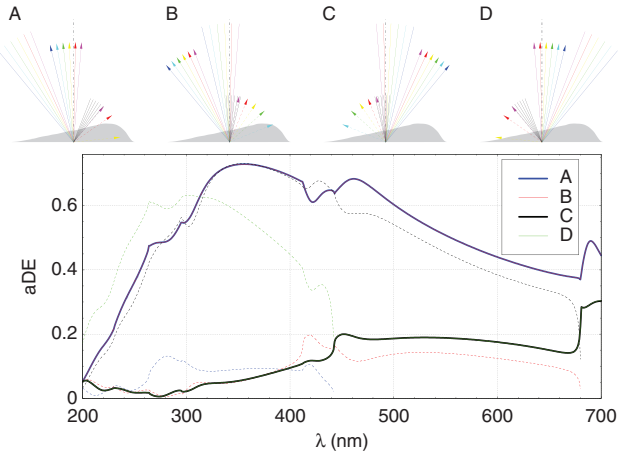

Figure 24 Four different possibilities to mount a 1180-l/mm monochromator grating *always* with 25.9° constant monochromator angle of deviation. Only the *left* mounting (A) corresponds to the application geometry. Colors from pink to red represent wavelengths from 240 nm to 740 nm in steps of 100 nm. *Long solid* and *short dashed* colored arrows indicate plus and minus first diffraction orders. Zero diffraction order is shown as short black line. Instead of tilting the grating to hit entrance and output port, the angle of incidence is varied, for picture drawing reasons only (*top*). The *bottom* graph shows related absolute diffraction efficiencies (aDE) into plus (*thick solid*) and minus (*thin dashed*) first diffraction order, simulated for the AFM profile shown in the *top* picture.

Mounting (A) and (B) in Figure 24 results in identical diffraction efficiencies for the plus first diffracted order, what is known as reciprocity theorem. This is not the case for the minus first diffracted order: e.g., for wavelengths longer than 680 nm in mounting (B), this order is evanescent. The same discussion is valid for mounting (C) and (D).

6.6 Influence of oxide depth

Again, there is a lot of literature concerning the influence of the aluminum oxide depth.

Typically, there is 3–6 nm of Al_2O_3 on top of an aluminum-coated grating. For gratings with high groove numbers as 3600 l/mm used in the UV region, there may occur large differences, and resonances may shift, as discussed above. Calculations are not shown here.

For a grating with small groove numbers, typically, the influence is less important, and UV efficiencies will simply drop by some percent. The influence of the aluminum oxide layer thickness is shown in Figure 25 for a 248-l/mm grating. The shorter the wavelength, the stronger the degradation of diffraction efficiency at this wavelength.

6.7 Perfect blazing

The term *perfect blazing* is used to describe the phenomenon that all incident energy is diffracted into one diffraction order (see Maréchal and Stroke [70]). For a long time, it was believed that perfect blazing cannot occur simultaneously for TE- and TM-polarized light. However, it was shown recently that perfect blazing may occur for TE- and TM-polarized light simultaneously [71].

7 Scattering and stray light

Scattering describes the diffuse redirection of light into nonspecular directions. *Stray light* includes any scattered light as well as specular ghost reflections.

Stray light inside a spectrometer limits its dynamics, resolution, and the correctness of the measured wavelength distributions. For optimizing a spectrometer's performance, the different sources of stray light should be identified *quantitatively* first. There is no need to invest large amounts of money for a high-end spectroscopic grating with minimal scattering as long as the

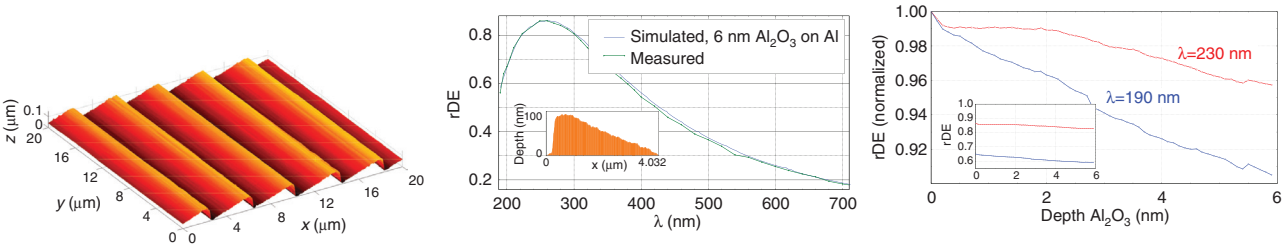

Figure 25 AFM picture of a 248-l/mm aberration-corrected blazed Carl grating, anamorphic scaled (*left*). Good match between measured and simulated relative diffraction efficiencies (rDE), inset shows the AFM-extracted profile with 1,86° blaze and 39° antiblaze angle, used for simulation (*center*). Normalized simulated diffraction efficiency over depth of aluminum oxide for two wavelengths, inset shows absolute (not normalized) values (*right*).

spectrometer stray light performance is dominated from specular ghosts or from scattered stray light by mechanical parts.

After minimizing all specular stray light and all scattering from mechanical surfaces inside the spectrometer, of course, the scattering of the high-end spectroscopic grating has to be characterized, too. To quantify the scattered light level of the grating, both *monochromatic* and *polychromatic* scattered light can be measured. The monochromatic scattered light is often characterized by measuring the *bidirectional scattering distribution function* (BSDF, see Nicodemus et al. [72]). The polychromatic scattered light is often measured in a grating configuration close to the application in the spectrometer (see ASTM E387-04). Both monochromatic and polychromatic scattered light depend on wavelength, angle of polar and azimuthal incidence, polarization, and scattered angle.

As mentioned above, the scattering of a grating represents the expertise of the manufacturer, and the quality of all materials used during IFL fabrication. To identify the influence of substrate and coating roughness as well as the influence of the quality of used aspheres, mirrors, light sources, pinholes, and many other elements, the surface roughness and the resulting scattered light distribution have to be characterized as well. For these unstructured surfaces, the *total integrated scatter* (TIS) value is often used to quantify the scattering. The TIS value is related to the surface roughness. The sum of transmitted, reflected, absorbed, and scattered light from a grating equals the incident light:

$$P_{\text{trans}} + P_{\text{refl}} + P_{\text{abs}} + P_{\text{sca}} = P_{\text{inc}},$$

as it is for any other surface, too.

At first, some typical specular ghost paths will be reviewed and also the scattering from mechanical surfaces. In the following, the scattering determined by the grating is shortly discussed.

7.1 Specular and scattered ghost paths

Some important origins of specular ghosts include the cover glass of the detector, mirror surfaces close to the detector, and unwanted diffraction orders. The cover glass will typically be antireflection (AR) coated. This AR coating reduces Fresnel losses. However, a non-negligible rest reflection from both surfaces remains. These reflexes can reach 1% or more if a broad wavelength range shall be addressed by the coating or high-index material as, e.g., sapphire or higher angles of incidence are used. Thus, a small part of the power, which is reflected back from the, e.g., Si- or InGaAs-detector, will be directly reflected back again to the detector – but not at the lateral position where this wavelength should hit. As a consequence, the signal is not only corrupted in amplitude but also wavelengths seem to occur, which do not exist in reality. The same problem occurs, if for some reason a mirror is located close to the detector. As this is a tutorial on gratings, not on spectrometers, these specular ghost paths shall not be discussed here in detail.

However, the influence of unwanted diffraction orders should be verified theoretically before releasing a new spectrometer design. Resulting from double diffraction inside the curved grating, this specular reflected stray light may hit the detector directly, as shown in Figure 26. For a quantitative estimation, the wavelength and angle dependence of all these diffraction orders have to be kept in mind.

Besides the scattered light from the grating, which will be discussed below, the scattered light from all other mechanical and optical parts of a spectrometer does contribute to the overall stray light, too. The smaller the spectrometer, the more difficult it is to minimize stray light. The resulting function, which shows the spectral answer of the spectrometer depending on a monochromatic input, is called the *signature*, as shown in Figure 27 before design optimization.

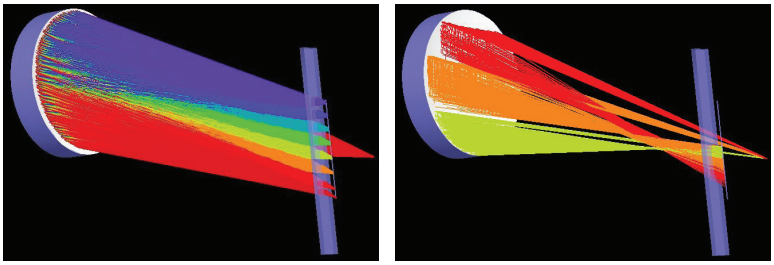

Figure 26 Only the desired diffraction into positive first diffracted order +1R is shown for eight wavelengths (*left*). Unwanted specular ghost paths occur for three of these eight wavelengths because of double diffraction into +2R first, and into -1R diffraction order directly after. All shown rays hit the detector (*right*).

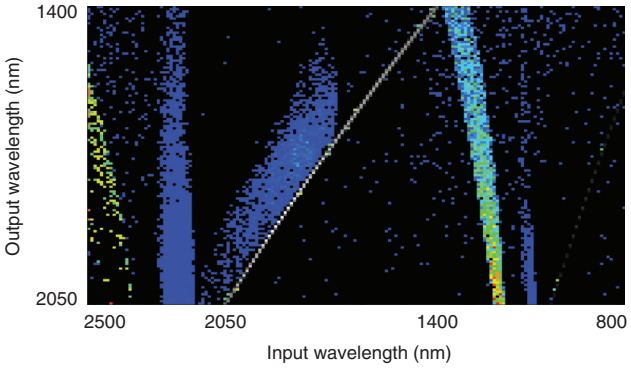

Figure 27 Simulated signature of a spectrometer before stray light optimization. Only the line of white dots from (1400 nm, 1400 nm) to (2050 nm, 2050 nm) should occur. Colored dots represent stray light from 10^{-7} to 10^{-2} in relation to this normalized power.

Of course, this device signature can be measured with an external monochromator feeding wavelength by wavelength, always evaluating the entire spectrum. However, it is advantageous to simulate this signature before passing the final spectrometer design, as the origin of different stray light hotspots can be found with little effort. If these hotspots on the detector are found, commercially available software, as, e.g., FRED [73], allows to present output path details or redraw the ray history (as was done to create Figure 26, *right*). This allows to quickly locate, e.g., a hundred rays (the origin of the hotspot) out of many millions and, thus, by eliminating this hotspot-origin, to improve the design of the spectrometer in an early stage.

7.2 Scattering from gratings

The term *scattering* can be used to describe all interactions of light and matter including diffraction, reflection, and transmission (see the *Ewald-Oseen* extinction theorem in Born and Wolf [4]). However, we will focus here only on the surface scattering of reflective (or also transmittive) gratings due to their finite surface roughness and groove profile imperfections.

Most relevant imperfections are random *groove spacing errors*, *groove depth errors*, and *surface microroughness*. Theoretically, groove spacing errors do not occur for gratings made by IFL. Practically, of course, the photoresist shows a granularity resulting in a finite groove number accuracy, and a finite groove depth accuracy. During the replication of a grating the profile changes in a statistical manner – on a nanoscale, we speak of groove spacing errors and groove depth errors of 1 nm and below. Typical measured BSDF values are shown in [74]. The already mentioned 'generation problem' does not only effect diffraction efficiency but also scattering. The BSDF of gratings from odd replication generations will group together and may differ from the BSDF of even generations.

Different *roughness* terms are used depending on the spatial frequencies analyzed. Surface height deviations measured on a lateral scale of a few micrometers or below are called *microroughness* and are measured typically with atomic force microscopy (AFM). Surface height deviations with lateral space frequencies on an order of about 1 μm^{-1} to about 1 mm^{-1} are called *roughness* and are measured typically with white light interferometry (WLI) using Mirau type objectives with different magnifications. Surface height deviations with lower space frequencies are called *waviness* or with even lower space frequencies *form* errors and are measured typically with (classical) optical interferometry.

The theoretical description and the measurement of scattering is already extensive for plane surfaces (see Stover [75]). A good introduction to the scattering of gratings can be found in [76]. Here, the different consequences for small angle (0.1°–1°) BSDF values near specular diffraction peaks, and for the achievable minimum of BSDF values in the middle between two diffraction orders,

depending on the above-mentioned imperfections, are discussed in detail. For mechanical ruled gratings, stronger imperfections owing to the ruling process will dominate, which will not be discussed here at all.

Mechanically ruled gratings are known to exhibit often a higher total level of scattered light compared to IFL written gratings. Mechanically ruled gratings have most of their scattered light in the meridional plane, which is not the case for IFL written gratings. For that reason, also the slit height in a spectrometer influences the stray light performance. The same grating, benchmarked once in a monochromator device and compared to the use in a polychromator device, may result in different stray light ratings.

Which of the above-mentioned imperfections dominate the overall scattering level of a grating, depends not only on technology but also strongly on groove number and groove depth. The different amounts may change with wavelength as scattered light strongly changes with it. During the replication process, the weighted contributions from the different imperfections may change, too.

8 Conclusions and outlook

Specifics in design and manufacturing of different grating types and grating mounts were compared. It was shown that Carl gratings with blazed grating profile have significant advantages for the application in high-end spectrometers. In particular, aberration correction for flatfield spectrometers allows miniaturization and, thus, the construction of lightweight handheld spectrometers without compromising resolution and SNR. With the focus on highest efficiencies and lowest scattered light level at the same time, challenges of IFL technology were discussed.

Spectroscopy development is mainly driven by the miniaturization of all components. There is a trend to smaller, lighter, flexible, configurable, and less expensive handheld mobile microspectrometers and miniaturized hyperspectral imagers with highest performance. The iSPEX add-on to a smartphone allows to measure aerosols in the atmosphere [77]. Handheld near-infrared spectrometers for food analysis are prophesied already for a long time. Highly promising fund-raising projects as TellSpec [78] successfully raised money, but seem not to match their promises. Consumer Physics, Tel Aviv, Israel [79] raised 2,7 Mio USD in 2014 for a revolutionary handheld device that tells you the allergens, chemicals, nutrients, calories, and ingredients in your food, but points out explicitly not to be a medical device. So, fortunately, it remains exciting.

Acknowledgments: The author gratefully acknowledges contributions of his colleagues M. Burkhardt, M. Cumme, A. Deparnay, H. J. Dobschal, A. Gatto, M. Helgert, R. Hultzsch, F. Koch, K. Rudolf, M. Schnabel, R. Steiner, G. Surowy, and all my colleagues from the grating manufacturing laboratory from Carl Zeiss Jena GmbH, and the inspiring discussions with them.

References

[1] D. Rittenhouse, Trans. Amer. Phil. Soc. 2, 201–206 (1786).
[2] G. W. Stroke, in 'Diffraction gratings', 'Handbuch der Physik', volume 29, Ed. By S. Flügge (Springer–Verlag, Berlin, Heidelberg, 1967) pp. 426–754.
[3] M. P. Chrisp, in 'Aberration-Corrected Holographic Gratings and Their Mountings', volume X (Academic Press, San Diego, 1987) pp. 391–454.
[4] M. Born and E. Wolf, in 'Principles of Optics', 6 edition (Cambridge University Press, Cambridge, 1997).
[5] E. G. Loewen and E. Popov, in 'Diffraction gratings and applications', (CRC Press, New York, 1997).
[6] O. Sandfuchs, C. Schwanke, M. Burkhardt, F. Wyrowski, A. Gatto, et al., J. Eur. Opt. Soc. 6, 11006 (2011).
[7] T. Glaser, S. Schröter, S. Fehling, R. Pöhlmann and M. Vlček, Electron. Lett. 40(3), 176–177 (2004).
[8] E. B. Burgh, M. A. Bershady, K. B. Westfall and K. H. Nordsieck, Publ. Astron. Soc. Pac. 119, 1069–1082 (2007).
[9] R. Brunner, M. Burkhardt, K. Rudolf and N. Correns, Opt. Exp. 16(16), 12239–12250 (2008).
[10] M. Burkhardt, R. Fechner, L. Erdmann, F. Frost, R. Steiner, et al., in 'DGaO-Proc, Erlangen-Nürnberg', 113, A3 (2012). ISSN: 1614 8436, URN:NBN:DE:0287 2012 A003 6.
[11] A. Gatto, A. Pesch, L. H. Erdmann, M. Burkhardt, A. Kalies, et al., in 'Sensors, Systems, and Next-Generation Satellites XVIII', Eds. By Pantazis Mouroulis and Thomas S. Pagano (SPIE, San Diego, 2014) pp. 1J–1.
[12] R. Hultzsch, Photonik (3), 40–41 (1998).
[13] C. G. Bernhard, Endeavour 26, 79–84 (1967).
[14] J. v. Fraunhofer. Versuche über die Ursachen des Anlaufens und Mattwerdens des Glases und die Mittel denselben zuvor zu kommen (1817, unpublished). Kunst- und Gewerbeblatt des Polytechnischen Vereins für das Königreich Bayern 52, 1–19 (1866).
[15] H. D. Taylor, A method of increasing the brillancy of the images formed by lenses, 1904. Patent No GB 29.561.
[16] A. Smakula, Verfahren zur Erhöhung der Lichtdurchlässigkeit optischer Teile durch Erniedrigung des Brechungsexponenten an den Grenzflächen dieser optischen Teile. Patent No DE 685767, 1. November 1935.
[17] M. J. Minot, J. Opt. Soc. Am. 66(6), 515–519 (1976).
[18] C. Morhard, C. Pacholski, D. Lehr, R. Brunner, M. Helgert, et al., Nanotechnology 21(42), 425301 (2010).
[19] M. Schulze, H.-J. Fuchs, E.-B. Kley and A. in 'MOEMS-MEMS 2008 Micro and Nanofabrication', Eds. By Thomas J. Suleski, Winston V. Schoenfeld and Jian J. Wang (SPIE, San Jose, 2008) pp. 68830N.

[20] T. Glaser, A. Ihring, W. Morgenroth, N. Seifert, S. Schröter, et al., Microsyst. Technol. 11(2–3), 86–90 (2005).
[21] ORAFOL, Fresnel Optics GmbH. http://www.orafol.com, 2014.
[22] R. Brunner and H. Dobschal, in 'Diffractive Optical Lenses in Imaging Systems – High-Resolution Microscopy and Diffractive Solid Immersion Systems', chapter 3 (Springer, Berlin, Heidelberg, 2007) pp. 45–70.
[23] R. Brunner, R. Steiner, K. Rudolf and H.-J. Dobschal, in 'Gradient Index, Miniature, and Diffractive Optical Systems III', SPIE 5177, 9–15 (2003).
[24] R. Brunner, Adv. Opt. Technol. 2(5–6), 351–359 (2013).
[25] C. V. Raman and N. S. N. Nath, Proc. Ind. Acad. Sci. (A) 2, 406–412 (1935).
[26] H. Kogelnik, Bell Sys. Tech. J. 48(9), 2909–2947 (1969).
[27] R. Extermann and G. Wannier, Helv. Phys. Acta 9, 520–532 (1936).
[28] M. A. Golub and A. A. Friesem, J. Opt. Soc. Am. A 24(3), 687–695 (2007).
[29] M. Rumpel, M. Moeller, C. Moormann, A. Voss, T. Graf, et al., in, Advanced Solid State Lasers ATh1A–7 (2013).
[30] J. Weiner, Rep. Prog. Phys. 72(064401), 1–19 (2009).
[31] T. Glaser, in 'Modeling Aspects in Optical Metrology', Eds. H. Bosse, B. Bodermann and R. M. Silver (SPIE, München, 2007) pp. 41.
[32] J. Dyson, J. Opt. Soc. Am. 49(7), 713–715 (1959).
[33] A. Offner, Unit power imaging catoptric anastigmat, 1973. US patent 3,748,015.
[34] L. Mertz, Appl. Opt. 16(12): 3122–3124, 1977.
[35] O. v. Littrow, Abtheilung 47(105), 26–32 (1863).
[36] A. Davis. Stray light in czerny-turner monochromators (master's degree paper). http://artdavis.wdfiles.com/local–files/optics-papers/Stray-light-in-Czerny-Turner-monochromators_Davis.pdf. see also: A. Davis and K. McNallie, US patent 6,414,753, 2002.
[37] P. H. A. Rowland, Philos. Mag. 13(84), 469–474 (1882).
[38] H. A. Rowland, Philos. Mag. 16(99), 210 (1883).
[39] C. Runge and F. Paschen, in 'Über die Strahlung des Quecksilbers im magnetischen Felde' (Berlin, Verlag der Königlichen Preussischen Akademie der Wissenschaften, 1902) pp. 1–18.
[40] A. Labeyrie and J. Flamand, Opt. Commun. 1(1), 5–8 (1969).
[41] R. Güther and S. Polze, Optica Acta, 29(5), 659–665 (1982).
[42] J. Cordelle, J. Flamand, G. Pieuchard and A. Labeyrie, in 'Aberration-Corrected Concave Gratings Made Holographically', (Oriel Press, Newcastle upon Tyne, 1970) pp. 117–124.
[43] R. Bittner, Optik 64(3), 185–199 (1983).
[44] O. Wiener, Ann. Phys. 276(6), 203–243 (1890).
[45] A. A. Michelson, Proc. Am. Philos. Soc. LIV(217), 137–142 (1915).
[46] R. Ritschl and S. Polze, Optik 15(2/3), 127–131 (1958).
[47] H. Nagata and M. Kishi, Jpn. J. Appl. Phys. 14(S1), 181–186 (1975).
[48] N. K. Sheridon, Appl. Phys. Lett. 12(9), 316–318 (1968).
[49] J. Flamand, F. Bonnemason, A. Thevenon and J. M. Lerner, in 'Raman Scattering, Luminescence and Spectroscopic Instrumentation in Technology', Eds. By Fran Adar, James E. Griffiths and Jeremy M. Lerner (SPIE, Los Angeles, 1989) pp. 288–294.
[50] M. Breidne, S. Johansson, L.-E. Nilsson and H. Åhlèn, Opt. Acta 26(11), 1427–1441 (1979).
[51] R. Fechner, A. Schindler, D. Hirsch, T. Gase, R. Weigelt, et al., in '10th Microoptics Conference MOC 04', (Springer, Jena, 2004) pp. F–16.
[52] P. Kröplin, Jenaer Jahrbuch zur Technik- und Industriegeschichte 170–209 (2000).
[53] D. W. Wilson, R. E. Muller, P. M. Echternach and J. P. Backlund, in 'Micromachining Technology for Micro-Optics and Nano-Optics III', Eds. E. G. Johnson, G. P. Nordin and T. J. Suleski, SPIE, San Jose, 5720, 68–77 (2005).
[54] M. Cumme and A. Deparnay, Adv. Opt. Technol. 4, 47–61 (2015).
[55] M. A. Gully-Santiago, D. T. Jaffe, C. B. Brooks, D. W. Wilson and R. E. Muller in 'Advances in Optical and Mechanical Technologies for Telescopes and Instrumentation', Eds. R. Navarro, C. R. Cunningham, and A. A. Barto, SPIE, 9151, 91515K–91515K–13, Montréal (2014).
[56] J. Fraunhofer, Ann. Phys. 74(8), 337–378 (1823).
[57] G. L. Turner and S. Bradbury, J. R. Microsc. Soc. 85(4), 435–447 (1966).
[58] B. H. Kleemann. Elektromagnetische Analyse von Oberflächengittern von IR bis XUV mittels einer parametrisierten Randintegralmethode: Theorie, Vergleich und Anwendungen. PhD thesis, Technische Universität Ilmenau, Germany (2002).
[59] PCGrate. http://www.pcgrate.com, 2014.
[60] unigit. http://www.unigit.com, 2014.
[61] JCMwave. http://www.jcmwave.com, 2014.
[62] WIAS-DiPoG. http://www.wias-berlin.de/software/DIPOG, 2014.
[63] VirtualLab. http://www.lighttrans.com, 2014.
[64] GSolver. http://www.gsolver.com, 2014.
[65] B. H. Kleemann, A. Mitreiter and F. Wyrowski, J. Mod. Opt. 43(7): 1323–1349 (1996).
[66] T. Glaser, S. Schröter, H. Bartelt, H.-J. Fuchs and E.-B. Kley, Appl. Opt. 41(18), 3558–3566, 2002.
[67] M. Breidne and D. Maystre, Appl. Opt. 19(11), 1812–1821 (1980).
[68] E. D. Palik. 'Handbook of optical constants of solids' (Academic Press, Boston, 1998).
[69] D. E. Gray. 'American Institute of Physics Handbook' (McGraw-Hill, New York, 1982).
[70] A. Maréchal and G. W. Stroke, C. R. Hebd. Séances Acad. Sci. 249(20), 2042–2044 (1959).
[71] B. H. Kleemann, Opt. Lett. 37(7), 1–3 (2012).
[72] F. E. Nicodemus, J. C. Richmond, J. J. Hsia, I. W. Ginsberg and T. Limperis, Geometrical considerations and nomenclature for reflectance. US Department of Commerce, National Bureau of Standards Washington, D. C (1977).
[73] FRED. http://photonengr.com, 2014.
[74] R. Steiner, A. Pesch, L. H. Erdmann, M. Burkhardt, A. Gatto, et al., in 'Imaging Spectrometry XVIII', Eds. by Pantazis Mouroulis and Thomas S. Pagano (SPIE, San Diego, 2013) pp. 0H–1.
[75] J. C. Stover, in 'Optical Scattering: Measurement and Analysis' (SPIE Optical Engineering Press, Bellingham, Washington, 3 edition, 2012).
[76] M. R. Sharpe and D. Irish, Opt. Acta 25(9), 861–893 (1978).
[77] F. Snik, J. H. Rietjens, A. Apituley, H. Volten, B. Mijling, et al., Geophys. Res. Lett. 41(20), 7351–7358 (2014).
[78] TellSpec. https://www.indiegogo.com/projects/tellspec-whats-in-your-food, 2013.
[79] Consumer Physics, Tel Aviv, Israel. https://www.consumerphysics.com/myscio/, 2014.

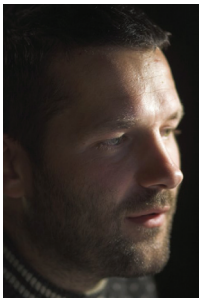

Tilman Glaser
Microstructured Optics/Grating Production,
Carl Zeiss Jena GmbH,
Carl-Zeiss-Promenade 10, 07745 Jena,
Germany
tilman.glaser@zeiss.com

Tilman Glaser is the head of the grating manufacture in the Carl Zeiss Jena GmbH, Jena, Germany. He studied at the Friedrich Schiller University (FSU) in Jena and at the Institut National des Sciences Appliquées (INSA) of Toulouse, France. He worked at the Institute for Physical High Technology IPHT in Jena in the area of grating design and manufacture from 1995 to 2004, and received his PhD degree in physics in 2000. From 2004 to 2007 he conducted research into multiple light beam light detection and ranging LIDAR systems for advanced driver assistance systems (ADAS) at Jenoptik LOS company. Since 2007 he has been working as a scientist in the microoptics group of the Zeiss company. His interests and experiences especially include design, fabrication and application of diffractive and refractive micro-optical elements.